NUMERICAL MODELLING OF THE ENDOTHERMIC PROCESS OF THE STEAM REFORMING OF METHANE IN A FIXED BED REFORMER

D. R. Dessaune,

V. F. Dias,

J. D. Silva,

Polytechnic School - UPE, Laboratory of Environmental and Energetic Technology; Rua Benfica - 455, Madalena, Recife - PE, Brazil, Cep: 50750-470

daniel.dessaune@gmail.com

vi.dias11@hotmail.com

jornandesdias@poli.br

ABSTRACT

Thermochemical Packed-Bed (TPB) reformer has been substantially studied in the past years as a promising equipment to investigate the thermochemical conversion of methane (CH_4). This work has as main objective a theoretical modelling to describe the process variables of Steam Reforming of Methane (SRM) method in the TPB reformer. The TPB reformer is filled with β-SiC open-cell foam where the thermochemical conversion of CH_4 is carried out. The model variables describe the specific aims of work and these objectives can be identified from each equation of the developed mathematical model. This work has been proposed to study two specific aims as (i) the effective thermal conductivity's effect of the solid phase ($\lambda_{s,eff.}$) and (ii) molar flows of chemical components. The endothermic reaction temperature's profiles are notably increased as the numeral value of $\lambda_{s,eff.}$ is raised. The Steam Reforming of Methane (SRM) method is suggested to improve the Production Rate (PR) of H_2 regarding the PR of CO. As results, the PR of H_2 is of 29.48% while the PR of CO is of 2.76%.

Keywords: β-SiC open-cell foam, TPB reformer, reaction temperature, SRM method, mathematical model

NOMENCLATURE

$C_{p, g, mix}$ Molar heat capacity at constant pressure of the gas mixture, kJ/kg K

$C_{p,s}$ Heat capacity pressure of the solid phase, kJ/kg K

$D_{ax, i}$ Dispersion coefficients of each component i, m^2/s

d_p Diameter of the solid particles, m

F_i Molar flow of components i, kmol/s

$F_{j,0}$ Initial molar flows of components j, kmol/s

g Gravity acceleration, m/s^2

h_{gs} Gas-solid heat transfer coefficient, W/m^2 K

k_{SRM} Reaction constant of the R_{SRM}, kmol $kPa^{0.5}/kg_{cat.}$ s

k_{WGSR} Reaction constant of the R_{WGSR}, kmol $kPa^{-1}/kg_{cat.}$ s

K_{SRM} Equilibrium constant of the R_{SRM}, kPa^2

K_{WGSR} Equilibrium constant of the R_{WGSR}

K_i Adsorption constants of components i, i = CO, H_2 and CH_4, kPa^{-1}

K_j Adsorption constant of components j, j = H_2O

L TPB reformer length, m

P_i Partial pressures of components i, i = CH_4, H_2O, CO, CO_2 and H_2, kPa

Pop. Operating pressure, kPa

q_g Gas phase's flow rate, m^3/s

r_i Net rates of components i (i = CH_4, H_2O, CO, CO_2 and H_2), kmol/$kg_{cat.}$ s

R_i Overall rates of the reforming reactions j, j = 1 and 2, kmol/$kg_{cat.}$ s

S_{sp} Spatial velocity, s^{-1}

t Iteration time, s

$T_{er, 0}$ Initial temperature of the endothermic reaction, K

T_{er} Temperature of the endothermic reaction, K

$T_{g, 0}$ Gas phase's initial temperature, K

T_g Gas phase's temperature, K

u_{sg} Gas superficial velocity, m/s

z Axial coordinate, m

Greek symbols

ε_b Packed-bed porosity, m^3 of gas/m^3 of reformer

ε_p Particle porosity, m^3 of particle/m^3 of reformer

η_i Effectiveness factors of reforming reactions j (j = SRM and WGSR)

$\lambda_{g,mix.}$ Gaseous mixture's thermal conductivity, W/m K

$\lambda_{g,eff.}$ Gas phase's effective thermal conductivity, W/m K

$\lambda_{s,eff.}$ Solid phase's effective thermal conductivity, W/m K

$\rho_{g,mix.}$ Gas mixture density of components I, kg/m^3

ρ_s Solid phase density, kg/m^3

INTRODUCTION

The production of hydrogen (H_2) can be carried out from different methods such as thermochemical (heat and chemical reactions to produce H_2),

reforming of hydrocarbons, biomass gasification, coal gasification, electrolytic, and biological (Lima et al., 2020; Anjos et al., 2020). The production of H_2 in packed bed reformers is still attracting the interest of researchers and engineers. Up to date, several works have been published in the literature dealing with reforming method to produce H_2 on different commercial catalyst (Silva and Abreu, 2017; Fuqiang et al., 2015; Yu et al., 2017). This work has as novelty the thermochemical conversion of CH_4 on a β-SiC open-cell foam in a Thermochemical Packed Bed (TPB) reformer. β-SiC open-cell foams have been considered as potential candidates for catalyst support in the heterogeneous catalysis field due to their high external surface area combined with a low pressure drop (Chen et al., 2018). On the other hand, foam-based packed bed reformers offer great potential advantages for the thermal energy storage due to bed's high porosity.

The hydrodynamic characterization of the Steam Reforming of Methane (SRM) through β-SiC open-cell foam in a packed bed configuration in the TPB reformer is performed by reacting Methane (CH_4) with water steam (H_2O). A physical-mathematical modelling is important to design and optimize the SRM method in the TPB reformer. Usually, the SRM method's application through β-SiC foam bed improves the heat transfer and mass transfer due to high porosity and surface area of the β-SiC foam (Vanhaecke et al., 2012). Mass, energy and momentum balance's equations for the gas phase as well as mass, energy and momentum balance's equations to the solid phase are described through mathematical models (Ma et al., 2016; Hussain et al., 2006). Here, a Non-isothermal Pseudo-Homogeneous Mathematical (NIPHM) model is used to model the SRM method in the TPB reformer. The NIPHM model is described by a system of Nonlinear Partial Differential Equations (NPDEs) in together with a developed kinetic model for reforming reactions.

With the purpose to reduce the research cost and project time, the mathematical modelling and computer simulation are extensively used to obtain a better understanding of design parameters in reformers. The approach and solution of physical-mathematical models are still a novelty of TPB reformers and thus the topic is a very actual in accessible literature. This work goal lies in the application of open-cell foam (β-SiC) bed for the SRM method. A numerical analysis has been driven to investigate the molar flows of chemical components i on the SRM method of the TPB reformer. In addition, the profiles of the endothermic reaction temperature were also analyzed for the SRM method in the TPB reformer.

PHYSICAL MODEL

A schematic setup is used to study the thermochemical conversion of the SRM method in TPB reformer according to Fig. 1. The physical model from TPB reformer is shown in Fig. 1.
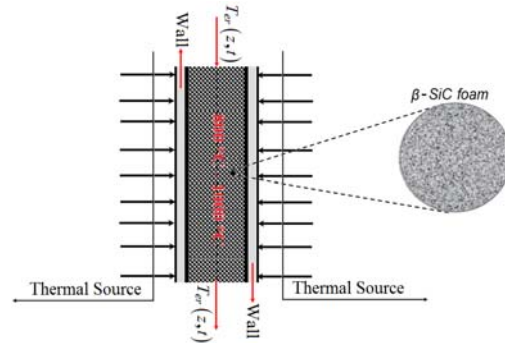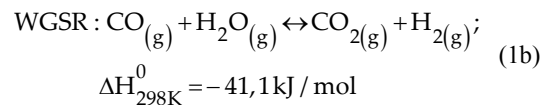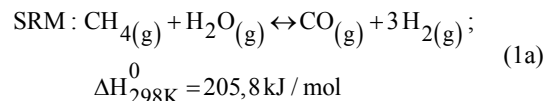

Figure 1. Schematic setup of the physical model from TPB reformer to study the SRM method on the β-SiC foam.

KINETIC MODEL

The reforming reaction of CH_4 is used to produce syngas (H_2 e CO) and it is highly endothermic (Cruz and Silva, 2017). On the other hand, the water-gas shift reaction (Eq. (1b)) is slightly exothermic and it is favoured at low temperatures. The SRM process has a limited equilibrium and can be described by the following reforming reaction:

$$SRM : CH_{4(g)} + H_2O_{(g)} \leftrightarrow CO_{(g)} + 3H_{2(g)};$$
$$\Delta H^0_{298K} = 205,8\,kJ/mol \tag{1a}$$

$$WGSR : CO_{(g)} + H_2O_{(g)} \leftrightarrow CO_{2(g)} + H_{2(g)};$$
$$\Delta H^0_{298K} = -41,1\,kJ/mol \tag{1b}$$

As Eq. (1a) is a highly endothermic reaction, then it needs to high temperatures to obtain great H_2 productivity. The overall rate equations of reactions, Eq. (1a) and Eq. (1b), are based on the Langmuir-Hinshelwood kinetic model and can be found in Ref. (Cruz and Silva, 2017). The kinetic rates from Eqs. (1a) and (1b) are considered more general for nickel (Ni) catalyst and, therefore, the equations of the SRM process is reported as:

$$R_{SRM} = \frac{\dfrac{k_{SRM}}{P_{H_2}^{2.5}}\left(P_{CH_4}P_{H_2O} - \dfrac{P_{H_2}^3 P_{CO}}{K_{SRM}}\right)}{\alpha^2} \tag{2a}$$

$$R_{WGSR} = \frac{\dfrac{k_{WGSR}}{P_{H_2}}\left(P_{CO}P_{H_2O} - \dfrac{P_{H_2}P_{CO_2}}{K_{WGSR}}\right)}{\alpha^2} \tag{2b}$$

where,

$$\alpha = 1 + \frac{F_{H_2O,0}}{F_{CH_4,0}} + \frac{F_{H_2,0}}{F_{CH_4,0}} + K_{CO}P_{CO} + K_{H_2}P_{H_2}$$
$$+ K_{CH_4}P_{CH_4} + \frac{K_{H_2O}P_{H_2O}}{P_{H_2}} \qquad (2c)$$

The partial pressures of chemical components i, i = CH_4, H_2O, CO, CO_2 and H_2 from Eqs. (2a)-(2c), are computed using Eqs. (3a)-(3e) as follows.

$$P_{CH_4} = \frac{1 - \left(1 - \frac{F_{CH_4}}{F_{CH_4,0}}\right)}{1 + \sum_j^4 \frac{F_{j,0}}{F_{CH_4,0}}} P_{op.} \qquad (3a)$$

$$P_{H_2O} = \frac{\frac{F_{H_2O,0}}{F_{CH_4,0}} - \left(1 - \frac{F_{CH_4}}{F_{CH_4,0}}\right) - \left(\frac{F_{CO_2}}{F_{CH_4,0}}\right)}{1 + \sum_j^4 \frac{F_{j,0}}{F_{CH_4,0}}} P_{op.} \qquad (3b)$$

$$P_{CO} = \frac{\frac{F_{CO,0}}{F_{CH_4,0}} + \left(1 - \frac{F_{CH_4}}{F_{CH_4,0}}\right) - \left(\frac{F_{CO_2}}{F_{CH_4,0}}\right)}{1 + \sum_j^4 \frac{F_{j,0}}{F_{CH_4,0}}} P_{op.} \qquad (3c)$$

$$P_{CO_2} = \frac{\frac{F_{CO_2,0}}{F_{CH_4,0}} + \left(\frac{F_{CO_2}}{F_{CH_4,0}}\right)}{1 + \sum_j^4 \frac{F_{j,0}}{F_{CH_4,0}}} P_{op.} \qquad (3d)$$

$$P_{H_2} = \frac{\frac{F_{H_2,0}}{F_{CH_4,0}} + 3\left(1 - \frac{F_{CH_4}}{F_{CH_4,0}}\right) - \left(\frac{F_{CO_2}}{F_{CH_4,0}}\right) - \frac{F_{H_2}}{F_{CH_4,0}}}{1 + \sum_j^4 \frac{F_{j,0}}{F_{CH_4,0}}} P_{op.} \qquad (3e)$$

$$j = H_2O, CO, CO_2 \text{ and } H_2$$

For the purpose of obtaining the net rates (r_i) to each chemical component i (i = CH_4, H_2O, CO, CO_2 and H_2), an expression is used to compute these net rates as follows.

$$r_i = \sum_{i=1}^5 \sum_{j=1}^2 \eta_j \, \sigma_{ij} R_j; \; j = SRM, WGSR \qquad (4)$$

In relation to the net rates, Eq. (4) is used to describe the net rate of each chemical component i of Eqs. (1a) and (1b) as follows.

$$r_{CH_4} = -\eta_{SRM} R_{SRM} \qquad (5a)$$

$$r_{H_2O} = -\left(\eta_{SRM} R_{SRM} + \eta_{WGSR} R_{WGSR}\right) \quad (5b)$$

$$r_{CO} = \eta_{SRM} R_{SRM} - \eta_{WGSR} R_{WGSR} \qquad (5c)$$

$$r_{H_2} = 3\eta_{SRM} R_{SRM} + \eta_{WGSR} R_{WGSR} \qquad (5d)$$

$$r_{CO_2} = \eta_{WGSR} R_{WGSR} \qquad (5e)$$

The kinetic constants, equilibrium constants and adsorption equilibrium constants for the calculations of reaction rates are described as a function of operating temperature (Cruz and Silva, 2017).

$$k_{SRM} = 2.636 \times 10^{13} \exp\left(-\frac{240.10}{R_u T_{op.}}\right) \qquad (6a)$$

$$K_{SRM} = 1.0267 \times 10^4 \exp\left(-\frac{26830.0}{T_{op.}}\right) + 30.114 \quad (6b)$$

$$k_{WGSR} = 12.194 \exp\left(-\frac{240.10}{R_u T_{op.}}\right) \qquad (6c)$$

$$K_{WGSR} = \exp\left(-\frac{26830.0}{T_{op.}}\right) - 4.063 \qquad (6d)$$

$$K_{CH_4} = 6.650 \times 10^{-6} \exp\left(-\frac{38.28}{R_u T_{op.}}\right) \qquad (6e)$$

$$K_{H_2O} = 1.770 \times 10^5 \exp\left(-\frac{88.68}{R_u T_{op.}}\right) \qquad (6f)$$

$$K_{H_2} = 6.120 \times 10^{-11} \exp\left(\frac{82.90}{R_u T_{op.}}\right) \qquad (6g)$$

$$K_{CO} = 8.230 \times 10^{-7} \exp\left(\frac{70.65}{R_u T_{op.}}\right) \qquad (6h)$$

MATHEMATICAL MODELLLING

The thermochemical modelling from TPB reformer are described by a NIPHM model. The development of the NIPHM model takes into account the following assumptions: (1) the NIPHM model is described under non-isothermal condition, (2) the NIPHM model from TPB reformer is plug-flow with axial dispersion under transient condition, (3) the radial dispersion is negligible inside TPB reformer, (4) the gaseous mixture has constant density in TPB reformer, (5) the molar flow rates inside TPB reformer are constant, (6) the deposition effect of carbon at the surface of catalytic particles has been neglected, (7) the gas behavior inside TPB reformer was considered as an ideal gas mixture, (8) the bed porosity in axial direction is considered constant, (9) the heaviest hydrocarbons than methane have not been considered in this work, and (10) chemical reactions as assumed to take place at the surface of catalyst particles. These premises are used to build the governing equations of the NIPHD model inside TPB reformer as follows.

GAS PHASE'S ENERGY BALANCE

A governing equation is described to study the heat distribution on the gas phase inside TPB

reformer. The proposed equation provides clear information to drive the temperature distribution on the gas phase under open-cell foam (β-SiC) bed. Therefore, a one-dimensional dynamic equation is developed for the gas phase's temperature as follows.

$$\rho_{g,mix.} C_{p,g,mix.} \left(\frac{\partial T_g}{\partial t} + \frac{4q_g}{\pi d_{refor.}^2} \frac{\partial T_g}{\partial z} \right) = \quad (7a)$$

$$\lambda_{g,eff} \frac{\partial^2 T_g}{\partial z^2} - h_{gs} \frac{(1-\varepsilon_b)}{\varepsilon_b} \frac{6}{d_p} \left(T_g - T_{er} \right)$$

The effective thermal conductivity of the gas phase is defined as a function of the gas thermal conductivity as follows.

$$\lambda_{g,eff.} = \varepsilon_b \lambda_{g,mix.} \quad (7b)$$

$$\lambda_{g,mix.} = 1.52 \times 10^{-11} T_{g,0}^3 - 4.86 \times 10^{-8} T_{g,0}^2 + \quad (7c)$$
$$1.02 \times 10^{-4} T_{g,0} - 3.93 \times 10^{-3}$$

The suitable initial and boundary conditions from Eq. (7a) are given as follows.

$$T_g \big|_{t=0} = T_{g,0} ; \ 0 \le z \le L \quad (7d)$$

$$\left. \frac{\partial T_g}{\partial z} \right|_{z=0^+} = \frac{\rho_{g,mix.} C_{p,g,mix.}}{\lambda_{g,mix.}} \frac{4q_g}{\pi d_{ref.}^2} \quad (7e)$$
$$\left(T_g \big|_{z=0^+} - T_{g,\infty} \right); \ t \ge 0$$

$$\left. \frac{\partial T_g}{\partial z} \right|_{z=L} = \frac{h_{gs,eff.}}{\lambda_{g,eff.}} \left(T_{g,\infty} - T_g \big|_{z=L} \right); \ t \ge 0 \quad (7f)$$

SOLID PHASE'S ENERGY BALANCE

The reactive packed-bed has been filled with β-SiC open-cell foams. The energy balance equation is built at the surface of β-SiC open-cell foams where take place the endothermic reaction of CH_4. The thermal storage takes place on the β-SiC open-cell foams to ensure sufficient energy to process the SRM's endothermic reaction. However, the energy balance for the SRM's temperature at the surface of β-SiC open-cell foams is given as follows.

$$\rho_s C_{p,s} \frac{\partial T_{er}}{\partial t} = \lambda_{s,eff} \frac{\partial^2 T_{er}}{\partial z^2} + h_{sg} \frac{6}{d_p} \frac{(1-\varepsilon_b)}{\varepsilon_b} \quad (8a)$$

$$\left(T_g - T_{er} \right) + \rho_s \frac{(1-\varepsilon_p)}{\varepsilon_p} \sum_{j=1}^{2} \pm \Delta H_j \eta_j R_j$$

The solid phase's thermal conductivity is defined as a function of the gaseous mixture's thermal conductivity according to Eq. (8b).

$$\lambda_{s,eff} = (1-\varepsilon_b) \lambda_{g,mix.} \quad (8b)$$

The suitable initial and boundary conditions from Eq. (8a) are given as follows.

$$T_{er} \big|_{t=0} = T_{er,0} ; 0 \le z \le L \quad (8c)$$

$$\left. \frac{\partial T_{er}}{\partial z} \right|_{z=0^+} = \frac{q_h}{\lambda_s}; \ t \ge 0 \quad (8d)$$

$$\left. \frac{\partial T_{er}}{\partial z} \right|_{z=L} = \frac{h_{sg,eff}}{\lambda_{s,eff.}} \left(T_{er,\infty} - T_{er} \big|_{z=L} \right); \ t \ge 0 \quad (8e)$$

TRANSPORT EQUATION OF CHEMICAL COMPONENTS

In Section TPB reformer's mathematical modelling, it was approached some assumptions that can be used to build the proposed problem's modelling. However, the transport equations for chemical components i (i = CH_4, H_2O, CO, CO and H_2) are presented as follows.

$$\frac{u_{sg}}{g} \frac{\partial F_i}{\partial t} + \frac{4q_g}{S_{sp} \pi d_{ref.}^2} \frac{\partial F_i}{\partial z} = \frac{D_{ax,i}}{S_{sp}} \frac{\partial^2 F_i}{\partial z^2} + \rho_s L \quad (9a)$$
$$r_{ref.}^2 \left(1-\varepsilon_b\right) r_i ; \ 0 < z < L$$

The suitable initial and boundary conditions for Eq. (9a) are presented as follows.

$$F_i \big|_{t=0,} = F_{i,0} ; \ 0 \le z \le L \quad (9b)$$

$$\left. \frac{\partial F_i}{\partial z} \right|_{z=0^+} = \frac{u_{sg} L}{\varepsilon_b D_{ax,i}} \left(F_i \big|_{z=0^+} - F_{i,\infty} \right); \ t \ge 0 \quad (9c)$$

$$\left. \frac{\partial F_i}{\partial z} \right|_{z=L} = \frac{k_{gs,eff} L}{\varepsilon_b D_{ax,i}} \left(F_i \big|_{z=L} - F_{i,\infty} \right); \ t \ge 0 \quad (9d)$$

PROPOSED MODEL'S SOLUTION BY CIEA

The CIEA's method can be employed as a good technique for studying the performance from TPB reformers (Dias and Silva, 2020). The CIEA's methodology has been used to transform the PDE system (Eqs. (7a), (8a), and (9a)) into an ODE system using the boundary conditions (Eqs. (7e), (7f), (8d), (8e), (9c) and (9d)) of each PDE. After transforming of PDEs into ODEs, the system of ODEs is reported as follows.

$$\alpha_{g,1}\frac{d\overline{T}_g(t)}{dt} = \left(\alpha_{g,2} - \lambda_{g,eff.}\,\alpha_{g,4}\right)T_g(0,t) -$$

$$\left(\alpha_{g,2} + \lambda_{g,eff.}\,\alpha_{g,5}\right)T_g(L,t) - \quad (10a)$$

$$\alpha_{g,3}\left(\overline{T}_g(t) - \overline{T}_s(t)\right) + \lambda_{g,eff.}$$

$$T_{g,\infty}\left(\alpha_{g,4} + \alpha_{g,5}\right)$$

$$\frac{d\overline{T}_{er}(t)}{dt} = \beta_{s,5}\left(\overline{T}_g(t) - \overline{T}_{er}(t)\right) - \beta_{s,1}\beta_{s,5}$$

$$T_{er}(L,t) + \beta_{s,1}\left(\beta_{s,5}\,T_{er,\infty} - \beta_{s,4}\right) \quad (10b)$$

$$+\sum_{j=1}^{2} \pm\Delta H_j\,\eta_j\,\overline{R}_j(t)$$

$$\frac{d\overline{F}_i(t)}{dt} = \left(\varphi_{f,2}\,\varphi_{f,5} - \varphi_{f,1}\right)F_i(L,t) - F_i(0,t)$$

$$\left(\varphi_{f,2}\,\varphi_{f,4} - \varphi_{f,1}\right) + \varphi_{f,3}\,\overline{r}_i(t) + F_{i,\infty} \quad (10c)$$

$$\varphi_{f,2}\left(\varphi_{f,4} - \varphi_{f,5}\right)$$

All coefficients from Eqs. (10a)-(10c) are presented in Appendices A, B and C, respectively.

FULL SOLUTION

The numeric methodology's choice is limited to the desired accuracy on the consistency and robustness of PDE system's numerical data (Cruz and Silva, 2017). In relation to ODEs of this work, Eqs. (10a) - (10c), they were solved by Runge-Kutta Gill method. On the other hand, the full solutions are approximated as follows.

$$T_g(z,t) = \frac{1}{2}T_g(z,t)\Big|_{t=0} + \sum_{k=1}^{\infty}\overline{T}_g(t_k)$$

$$\sin\left(\frac{k\pi z}{L}\right) \quad (11a)$$

$$T_{er}(z,t) = \frac{1}{2}T_{er}(z,t)\Big|_{t=0} + \sum_{k=1}^{\infty}\overline{T}_{er}(t_k)$$

$$\sin\left(\frac{k\pi z}{L}\right) \quad (11b)$$

$$F_i(z,t) = \frac{1}{2}F_i(z,t)\Big|_{t=0} + \sum_{k=1}^{\infty}\overline{F}_i(t_k)$$

$$\sin\left(\frac{k\pi z}{L}\right) \quad (11c)$$

RESULTS AND DISCUSSIONS

In the mathematical model, a physical-mathematical modelling has been developed to investigate the SRM method in the TPB reformer. A computational algorithm using the FORTRAN 95 has been elaborated by authors to compute the SRM method's variables in the TPB reformer.

KINETIC PARAMETERS

In section of the physical model of this work, kinetic model's equations were presented. The kinetic model's parameters are used to feed the computational algorithm in combination with hydrodynamic model's parameters from the TPB reformer. The numerical values of the kinetic model's parameters are shown in Table 1 below:

Table 1. Kinetic constants of reactions, equilibrium constants of reactions and adsorption constants

Parameters	Values	Sources
k_{SRM} (mol (kPa)$^{0.5}$ /kgcat. s)[1]	2.015×10^{11}	Eq. (6a)
K_{SRM} (kPa)^2 [1]	2.135×10^7	Eq. (6b)
K_{WGSR} (mol (kPa)$^{-1}$/kg$_{cat.}$ s) [1]	1.218×10^3	Eq. (6c)
K_{WGSR} (-) [1]	13.015	Eq. (6d)
K_{CH4} (kPa)$^{-1}$ [1]	8.974×10^{-7}	Eq. (6e)
K_{H2O} (-) [1]	3.701×10^4	Eq. (6f)
K_{H2} (kPa)$^{-1}$ [1]	8.987×10^{-12}	Eq. (6g)
K_{CO} (kPa)$^{-1}$ [1]	5.671×10^{-6}	Eq. (6h)
η_{SRM} (-) [1]	0.021	Cruz and Silva, 2017
η_{WGSR} (-) [1]	0.0169	Cruz and Silva, 2017

[1] Computed at 900°C

MODEL PARAMETERS

In Tables 2 and 3, operating conditions and hydrodynamics parameters have been presented. Table 2 shows the operating conditions of TPB reformer as well as bed properties of this reformer On the other hand, Table 3 reports thermophysical properties, inlet molar flow of components and dispersion coefficients of chemical components.

Table 2. Operating conditions and bed properties for the TPB reformer.

Model parameters	Values	Source
L (m)	0.60	Estimated
d_p (m)	3.4×10^{-4}	Estimated
$d_{refor.}$ (m)	3.2×10^{-3}	Estimated
$T_{g,0}$ (K)	673	Estimated
$T_{er,0}$ (K)	673	Estimated
$P_{op.}$ (kPa)	600	Estimated
q_g (m^3/s)	1.201×10^{-6}	Estimated
g (m/s^2)	9.81	Estimated
Sp (s^{-1})	3.53×10^7	Cruz and Silva, 2017
ε_b (m^3 of gas/m^3 of reformer)	0.39	Dias and Silva, 2020
ε_p (m^3 of gas/m^3 of reformer)	0.87	Voltolina et al., 2017

Table 3. Thermophysical properties, inlet molar flow of components and dispersion parameters for the SRM process.

Model parameters	Values	Source
$\rho_{g,\ mix.}$ (kg/m^3)	0.1692	Silva and Abreu, 2016
$C_{p,\ g,\ mix.}$ (kJ/kg K)	127.09	Dias and Silva, 2020
$\lambda_{g,\ eff}$ (W/m K)	1.078	Eq. (7b)
h_{gs} (W/m^2 K)	1.902	Dias and Silva, 2020
$C_{p,\ s}$ (J/kg K)	336.00	Dias and Silva, 2020
$\lambda_{s,\ eff}$ (W/m K)	0.501	Eq. (6b)
$F_{CH4,0}$ (mol/s)	0.25	Silva and Abreu, 2016
$F_{H2O,0}$ (mol/s.)	0.75	Silva and Abreu, 2016
$F_{H2,0}$ (mol/s)	7.62×10^{-5}	Silva and Abreu, 2016
$F_{CO,0}$ (mol/s)	3.2×10^{-5}	Silva and Abreu, 2016
$F_{CO2,0}$ (mol/s)	6.32×10^{-5}	Silva and Abreu, 2016
$D_{ax,\ CH4}$ (m^2/s) [1]	289×10^{-3}	Cruz and Silva, 2017
$D_{ax,\ H2O}$ (m^2/s) [1]	3.79×10^{-3}	Cruz and Silva, 2017
$D_{ax,\ H2}$ (m^2/s) [1]	2.01×10^{-3}	Cruz and Silva, 2017
$D_{ax,\ CO}$ (m^2/s) [1]	3.41×10^{-3}	Cruz and Silva, 2017
$D_{ax,\ CO2}$ (m^2/s) [1]	1.89×10^{-3}	Cruz and Silva, 2017

[1] Computed at 900°C

VALIDATION AGAINST PUBLISHED DATA

To ensure the validity of the proposed model, authors have made a comparison of simulated results with published data of the literature. The simulating results are computed from a computer code developed by authors. Slight differences can be found due to the deviation between the literature results and simulating results. An average relative error (ARE), Eq. (12a), was used to compute the consistency criterion and therefore, the ARE is given as follows.

$$ARE = \left| \frac{F_i^{Exp.\ results} - F_i^{Simul.\ results}}{F_i^{Exp.\ results}} \right| x\ 100; \qquad (12a)$$

$$i = CH_4, H_2O, H_2, CO\ and\ CO_2$$

Fig. 2 compares the literature results and simulated results of molar flows of chemical components i at the outlet of the TPB reformer. The good agreement between the simulated results and literature data reports that the developed model is acceptable. As it can be seen in Fig. 2, the simulated

results against the experimental results from literature (Chompupun et al., 2018) have presented a good agreement, resulting in AREs of ARE_{CH4} = 9.28%, ARE_{H2O} = 0.81%, ARE_{H2} = 1.29%, ARE_{CO} = 9.74%, and ARE_{CO2} = 2.13%. These AREs should be due to the incompatibility between the simulating results and experimental results.
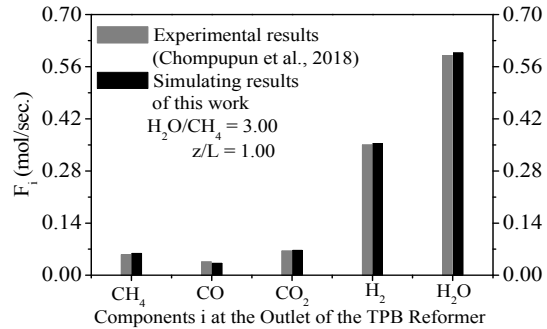

Figure 2. Comparison between molar flows of chemical components i at the outlet of TPB reformer.

NUMERICAL EXPERIMENTS

The profiles of the Endothermic Reaction Temperature (ERT) were computed from Eq. (20) for the SRM method in the TPB reformer. In Fig. 3, it is checked the dynamic region and stationary region along the TPB reformer's length. The dynamic region occurs up to ± 0.18 m, after that the stationary state is kept until 0.60 m. It was reported that the profiles of the endothermic reaction temperature tend to assume an inflection point at minimum values because of the endothermic reaction's effect. The range of the $\lambda_{s,\ eff}$ has a pertinent effect on the ERT's profiles in TPB reformer. Three different values of the $\lambda_{s,\ eff}$ have been used to check the ERT's sensibility to the $\lambda_{s,\ eff}$. As results, when the $\lambda_{s,\ eff}$ is higher ($\lambda_{s,\ eff}$ = 129.23), the heat absorption in TPB reformer is notably increased and therefore, the ERT's profile is favored. On the other hand, when the $\lambda_{s,\ eff}$ is lower ($\lambda_{s,\ eff}$ = 107.26), the heat absorption in TPB reformer is remarkably decreased and thus, the ERT's profile is reduced.
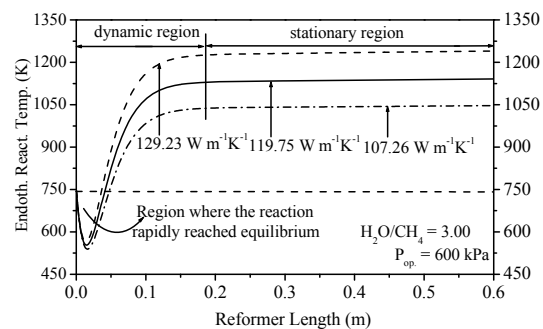

Figure 3. Endothermic reaction temperature's profiles along of the TPB reformer's length on β-SiC foam.

Fig. 4 shows the profiles of the molar flow of each chemical component i of the SRM method at the following operating conditions: $H_2O/CH_4 = 3.00$, 500 kPa, 1173 K, and 1.201×10^{-6} (m³/s). In this figure, the profiles of the molar flows from the consumed reactants (H_2O and CH_4) and produced products (CO, CO_2 and H_2) are reported in the TPB reformer. After reaching the stable state, only 18.67% of H_2O was consumed. On the other hand, after achieving the stable state, 97.26% of CH_4 was consumed. After reaching the stable state, 29.48% of H_2, 14.23% of CO_2, and 2.76% of CO were produced for the SRM method in the TPB reformer.
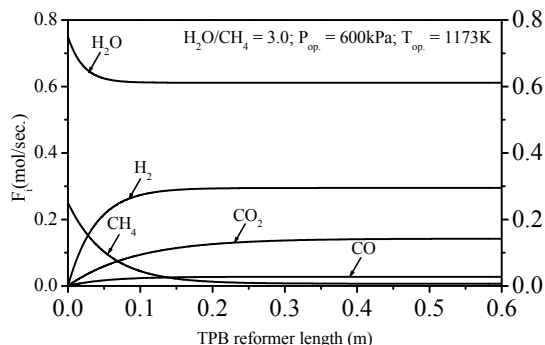

Figure 4. Molar flows of each chemical component i along of the TPB reformer's length on β-SiC foam.

CONCLUSIONS

A non-isothermal pseudo-homogeneous mathematical model which includes the thermal energy transfer on the endothermic thermochemical conversion and mass transfer coupled with a thermochemical kinetic model was developed and validated against published data of the literature for a TPB reformer. After validating the numerical model, such model can be used like a process simulator. Therefore, the major conclusions are listed as follows.

1. The simulating results of molar flows are similar to experimental results of molar flows under same operating conditions. The validating results have driven a good agreement against the literature data for molar flows at the outlet from TPB.
2. When the $\lambda_{s, eff.}$ is notably increased, the ERT's profile is raised. On the other hand, when the $\lambda_{s, eff.}$ is remarkably reduced, the ERT's profile is decreased.
3. Under the prescribed operating conditions, 18.67% of H_2O and 97.26% of CH_4 were consumed while 29.48% of H_2, 14.23% of CO_2, and 2.76% of CO were produced.

ACKNOWLEDGEMENTS

REFERENCES

Anjos E. B., Silva Filho A. M., Silva J. D., 2020, Numerical simulation of the steam reforming of toluene in a fixed-bed catalytic reformer to produce hydrogen, J Braz. Soc. Mech. Sci. Eng, Vol 42, 114.

Chen, X., Fuqiang, W., Han, Y., Yu, R., Cheng, Z., 2018, Thermochemical storage analysis of the dry reforming of methane in foam solar reactor, Energy Conversion and Management, Vol. 158, pp. 489-498.

Chompupun, T., Limtrakul, S., Vatanatham, T., Kanhari, C., Ramachandran, P. A., 2018, Experiments, modeling and scaling-up of membrane reformers for hydrogen production via steam methane reforming, Chemical Engineering Processing, Vol. 134, pp. 124-140.

Cruz, B. M., Silva, J. D., 2017, A two-dimensional mathematical model for the catalytic steam reforming of methane in both conventional fixed-bed and fixed-bed membrane reformers for the production of hydrogen, International Journal of Hydrogen Energy, Vol. 42, 23670-23690.

Dias, V. F., Silva, J. D., 2020, Mathematical modelling of the solar - driven steam reforming of methanol for a solar thermochemical micro - fluidized bed reformer: thermal performance and thermochemical conversion, Braz. Soc. Mech. Sci Eng., Vol. 42, pp. 447.

Fuqiang, W., Zhennan, G., Jianyu, T., Zhenyu, Y., Yu, L., 2015, Unsteady state thermochemical performance analyses of solar driven steam methane reforming in porous medium reactor, Solar Energy, Vol. 122. Pp. 1180-1192.

Hussain, A., Seidel-Morgenstern, A., Tsotsas, E., 2006, Heat and mass transfer in tubular ceramic membranes for membrane reformers, International Journal of Heat Mass Transfer, Vol. 49, pp. 2239-2253.

Ma, Y., He, L., Li, S., Teng, J., 2016, Heat transfer of oil shale in a small-scale fixed bed, Journal of Thermal Analysis and Calorimetry, Vol.124, pp. 461-469.

Lima, K. P. M., Dias, V. F. and Silva, J. D., 2020, Numerical modelling for the solar driven bi-reforming of methane for the production of syngas in a solar thermochemical micro-packed bed reformer, International Journal of Hydrogen Energy, Vol. 45, pp. 10353-10369.

Silva, J. D. and Abreu, C. A. M., 2016, Modelling and simulation in conventional fixed-bed and fixed-bed membrane reformers for the steam reforming of methane, International Journal of Hydrogen Energy, Vol. 41, pp. 11669-11674.

Vanhaecke, C., Pham-Huu, C., Edouard, D., 2012, Simulation and experimental measurement of

dynamic behavior of solid foam filter for diesel exhaust gas, Catalysis Today, Vol. 189, pp. 101-110.

Voltolina, S., Marín, P., Díz, F. V., Salvador, O., 2017, Open-cell foams as beds in multiphase reactors: Residence time distribution and mass transfer, Chemical Engineering Journal, Vol. 316, pp. 323 - 331.

Yu, T., Yuan, Q., Lu, J., Ding, J. Lu, Y., 2017, Thermochemical storage performances of methane reforming with carbon dioxide in tubular and semi-cavity reactors heated by a solar dish system, Applied Energy, Vol. 185, pp.1994-2004.

Appendix A: Coefficients from Eq. (10a)

$$\alpha_{g,1} = \rho_{g,mix.}\, C_{p,g,mix.} \tag{A.1}$$

$$\alpha_{g,2} = \rho_{g,mix.}\, C_{p,g,mix.}\, \frac{4\,q_g}{\pi\, d_{rz}^2} \tag{A.2}$$

$$\alpha_{g,3} = h_{gs}\, \frac{(1-\varepsilon_b)}{\varepsilon_b}\, \frac{6}{d_p} \tag{A.3}$$

$$\alpha_{g,4} = \frac{\rho_{g,mix.}\, C_{p,g,mix.}}{\lambda_{g,mix.}} \tag{A.4}$$

$$\alpha_{g,5} = \frac{h_{gs,eff.}}{\lambda_{g,eff.}} \tag{A.5}$$

$$\lambda_{g,1} = \frac{L\left(6 + L\,\alpha_{g,5}\right)\left(1 + 0.5\,L\,\alpha_{g,4}\right)}{1 + 0.5\,L\,\alpha_{g,5}} \tag{A.6}$$

$$\alpha_{g,6} = L\left(6 + L\,\alpha_{g,4}\right) - \lambda_{g,1} \tag{A.7}$$

$$\lambda_{g,2} = L^2\left(\alpha_{g,4}\, T_{g,\infty}^{Up.} + \alpha_{g,5}\, T_{g,\infty}^{Bot.}\right) \tag{A.8}$$

$$\alpha_{g,7}(t) = 12\,\overline{T}_g(t) + \lambda_{g,2}\left(1 + \frac{3 + 0.5\,L\,\alpha_{g,5}}{1 - 0.5\,L\,\alpha_{g,5}}\right) \tag{A.9}$$

$$T_g(0,t) = \frac{\alpha_{g,7}(t)}{\alpha_{g,6}} \tag{A.10}$$

$$\lambda_{g,3} = \frac{0.5\,L\,T_{g,\infty}\left(\alpha_{g,4} + \alpha_{g,5}\right)}{1 - 0.5\,L_z\,\alpha_{g,5}} \tag{A.11}$$

$$T_g(L,t) = \lambda_{g,3} - \frac{\left(1 + 0.5\,L\,\alpha_{g,4}\right)\alpha_{g,7}(t)}{\alpha_{g,6}\left(1 - 0.5\,L_z\,\alpha_{g,5}\right)} \tag{A.12}$$

Appendix B: Coefficients from Eq. (10b)

$$\beta_{s,1} = \frac{\lambda_{s,eff.}}{\rho_s\, C_{p,s}} \tag{B.1}$$

$$\beta_{s,2} = h_{sg}\, \frac{6}{d_p}\, \frac{1}{\rho_s\, C_{p,s}}\, \frac{(1-\varepsilon_b)}{\varepsilon_b} \tag{B.2}$$

$$\beta_{s,3} = \frac{(1-\varepsilon_p)}{\varepsilon_p} \tag{B.3}$$

$$\beta_{s,4} = \frac{q_h}{\lambda_s} \tag{B.4}$$

$$\beta_{s,5} = \frac{h_{sg,eff.}}{\lambda_{s,eff.}} \tag{B.5}$$

$$\beta_{s,6} = 2\,L\left(3 - \frac{6 + L\,\beta_{s,5}}{2 + L\,\beta_{s,5}}\right) \tag{B.6}$$

$$\vartheta_{s,1} = L^2\left(\beta_{s,4} - \beta_{s,5}\, T_{er,\infty}\right) \tag{B.7}$$

$$\vartheta_{s,2} = \frac{L^2\left(6 + L\,\beta_{s,5}\right)\left(\beta_{s,4} + \beta_{s,5}\, T_{er,\infty}\right)}{2 + L\,\beta_{s,5}} \tag{B.8}$$

$$\beta_{s,7}(t) = 12\,\overline{T}_{er}(t) - \vartheta_{s,1} - \vartheta_{s,2} \tag{B.9}$$

$$T_{er}(0,t) = \frac{\beta_{s,7}(t)}{\beta_{s,6}} \tag{B.10}$$

$$\vartheta_{s,3} = L\left(\beta_{s,4} + \beta_{s,5}\, T_{er,\infty}\right) + \frac{2\,\beta_{s,7}(t)}{\beta_{s,6}} \tag{B.11}$$

$$T_{er}(L,t) = \frac{\vartheta_{s,3}}{2 + L\,\beta_{s,5}} \tag{B.12}$$

Appendix C: Coefficients from Eq. (10c)

$$\varphi_{f,1} = \frac{4\,q_g}{S_{sp}\,\pi\, d_{ref.}^2}\, \frac{g}{u_{sg}} \tag{C.1}$$

$$\varphi_{f,2} = \frac{g}{u_{sg}}\, \frac{D_{ax.,i}}{S_{sp}} \tag{C.2}$$

$$\varphi_{f,3} = \frac{g}{u_{sg}}\, \rho_s\, r_{ref.}^2\, L\left(1-\varepsilon_b\right) \tag{C.3}$$

$$\varphi_{f,4} = \frac{L}{\varepsilon_b}\, \frac{u_{sg}}{D_{ax.,i}} \tag{C.4}$$

$$\varphi_{f,5} = \frac{L}{\varepsilon_b}\, \frac{k_{sg}}{D_{ax.,i}} \tag{C.5}$$

$$\upsilon_{f,1} = \frac{L\left(6 - L\,\varphi_{f,5}\right)}{2 - L\,\varphi_{f,5}}\left(2 + L\,\varphi_{f,4}\right) \tag{C.6}$$

$$\varphi_{f,6} = L\left(6 + L\,\varphi_{f,4}\right) - \upsilon_{f,1} \tag{C.7}$$

$$\upsilon_{f,2} = L^2\, F_{i,\infty}\left(\varphi_{f,5} - \varphi_{f,4}\right) \tag{C.8}$$

$$\upsilon_{f,2} = \frac{L^2\, F_{i,\infty}\left(6 - L\,\varphi_{f,5}\right)\left(\varphi_{f,4} + \varphi_{f,5}\right)}{2 - L\,\varphi_{f,5}} \tag{C.9}$$

$$\varphi_{f,7}(t) = 12\,\overline{F}_i(t) - \upsilon_{f,2} - \upsilon_{f,3} \qquad \text{(C.10)}$$

$$F_i(0,t) = \frac{\varphi_{f,7}(t)}{\varphi_{f,6}} \qquad \text{(C.11)}$$

$$\upsilon_{f,4} = \left(2 + L\,\varphi_{f,4}\right)\frac{\varphi_{f,7}(t)}{\varphi_{f,6}} \qquad \text{(C.12)}$$

$$\upsilon_{f,5} = L\,F_{i,\infty}\left(\varphi_{f,4} + \varphi_{f,5}\right) \qquad \text{(C.13)}$$

$$F_i(L,t) = \frac{\left(\upsilon_{f,4} - \upsilon_{f,5}\right)}{2 - L\,\varphi_{f,5}} \qquad \text{(C.14)}$$